


**Hydrodynamic interactions between swimming microorganisms in a linearly density stratified fluid**Rishabh V. More  and Arezoo M. Ardekani \**School of Mechanical Engineering, Purdue University, West Lafayette, Indiana 47907, USA* (Received 13 July 2020; revised 16 October 2020; accepted 1 December 2020; published 20 January 2021)

Oceans and lakes sustain intense biological activity due to the motion of marine organisms, which has significant ecological and environmental impacts. The motion of individual organisms and their interactions with each other play a significant role in the collective motion of swimming organisms. However, ubiquitous vertical density stratification in these aquatic environments significantly alters the swimmer interactions as compared to in a homogeneous fluid. Furthermore, organisms have sizes varying over a wide range which results in finite inertia. To this end, we numerically investigate the interactions between a pair of model swimming organisms in two configurations: (1) approaching each other and (2) moving side by side with finite inertia in a linearly density stratified fluid. We use the archetypal reduced-order squirmer model to numerically model the swimming organisms. We present trajectories and the contact times of interacting squirmer (puller & pusher) pairs for different  $Re$  in the range 1–50 and  $Ri$  in the range 0–10. Depending on the squirmer  $Re$  and  $Ri$  we observe that the squirmer interactions can be categorized as (i) pullers getting trapped in circular loops at high  $Re$  and low  $Ri$ , (ii) pullers escaping each other with separating angle decreasing with increasing stratification at low  $Re$  and high  $Ri$ , (iii) pushers sticking to each other after the collision and deflecting away from the collision plane for either low  $Re$  or high  $Ri$ , (iv) pushers escaping otherwise with an angle of separation increasing with stratification. Stratification also increases the contact time for squirmer pairs. The presented results can be useful to understand the mechanisms behind the accumulation of planktonic organisms in horizontal layers in a stratified environment such as oceans and lakes.

DOI: [10.1103/PhysRevE.103.013109](https://doi.org/10.1103/PhysRevE.103.013109)**I. INTRODUCTION**

The sizes of swimming organisms span a wide range of length scales, from micrometers to a few meters. Thus, depending on their size, these organisms employ a variety of swimming mechanisms that take advantage of the fluid flow around them to propel themselves. In a fluid with a characteristic density  $\rho_0$  and dynamic viscosity  $\mu$ , the Reynolds number for an organism of size  $a$  and moving with a speed  $U_0$  is defined as  $Re = \rho_0 U_0 a / \mu$ , which is the ratio of inertial to viscous forces. At microscales,  $Re \approx 0$  and the microorganisms make use of the viscous drag exerted by the fluid to move. Larger organisms such as fishes and whales have a finite  $Re$  and utilize the lift generated by the fluid accelerating past them to swim.

In recent years, researchers have devoted significant effort to investigate the collective dynamics of organisms. Dense suspensions of bacteria on scales much larger than a cell in the Stokes flow limit exhibit transient, reconstituting, high-speed jets straddled by vortex streets [1], self-sustained turbulence [2], extended spatiotemporal coherent dynamics [3], and superdiffusion in short times [4]. The collective motion of the bacteria is determined by short-range pair interactions at high concentrations [2]. Even at high  $Re$ , e.g., schooling fish, flocking birds, and swarming insects, the hydrodynamic interaction between the moving organisms and their detached vortical

structures significantly affect the swimming (flying) efficiency [5,6].

Many studies of the collective behavior of swimmers neglect the near-field hydrodynamic interactions and only consider the far-field interactions to simulate the dynamics of swimmer suspensions [7,8]. But, to completely understand the collective behavior of the microswimmers, it is important to investigate the near-field hydrodynamics between a pair of interacting swimmers. It is well known that in the dilute limit, microswimmers behave as a force dipole, leading to a velocity field decaying as  $1/r^2$ , where  $r$  is the distance from the microswimmer [9]. Due to the slow decay of the induced velocity field, the pairwise interaction between two swimmers cannot be neglected, even at large separations. Various experimental studies have shown the crucial role of hydrodynamic interactions between microorganisms in determining their dynamics, e.g., dancing *Volvox* [10], interacting pair of *Paramecia* [11], the formation of dynamic clusters in suspensions of motile bacteria [12], and hydrodynamic self-mediation of bacteria into two-dimensional crystals [13].

Many theoretical and numerical studies have also been conducted to investigate the hydrodynamic interactions between two model swimmers. Pullers (pulled from the front) are attracted towards each other first, which leads to near contact and changes in their swimming orientations to finally separate [14,15]. Two self-propelling bacteria by rotating helical flagella avoid each other by changing their orientations [16]. The swimmer-swimmer interaction is complex and strongly affected by their relative displacement, orientation,

\*ardekani@purdue.edu.

initial configuration, and swimming stroke phase. Slight variations in these parameters lead to different scattering angles, swimming speeds, and a range of different interactions, such as attraction, repulsion, or oscillation [17–20]. Hydrodynamic interactions between two microswimmers also lead to the enhancement of the swimming efficiency by synchronizing the phase of two adjacent flagella [21]. However, all of these studies were performed in the Stokes regime assuming  $Re = 0$  without considering the effect of swimmer inertia.

For swimming microorganisms, the  $Re$  ranges from  $10^{-4}$  for bacteria [22],  $10^{-3}$  for *Chlamydomonas*, 0.01–0.1 for *Volvox* [10], 0.1–1 for freely swimming zooplankton *Daphnia magna* [23], 0.2–2 for *Paramecia* depending on swimming or escaping mode [11],  $O(10)$  for *Pleurobrachia*, and 20–150 for copepods [24]. Thus, it is crucial to know the influence of finite inertia on the hydrodynamic interactions of two swimmers. Theoretical and computational studies on the locomotion of an individual swimmer with finite inertia [25,26] further indicate that inertia can lead to notable differences in the swimming dynamics of swimmers. Inertia also affects the hydrodynamic interactions between swimmer pairs. Puller and pusher pairs either separate away from each other or get trapped near each other depending on their  $Re$  and swimming modes [27].

Many swimming organisms with low to intermediate  $Re$  are abundant in oceans and lakes and their motion results in intense biological activity in these aquatic bodies. Hence, studying the interactions of organisms is an intriguing problem having wide implications for ocean ecology [28]. However, understanding the physics behind these phenomena is a complex undertaking as vertical variations in water density are ubiquitous in aquatic and marine environments [29] due to gradients in temperature (thermoclines) or salinity (haloclines). These density variations with depth can manifest themselves in a gamut of environmental and oceanographic processes [30–33]. Even though the stratification length scale is  $O(m)$ , the appropriate length scale to determine whether stratification affects the motion of the swimmers is  $O(100) \mu\text{m}$  [34]. Marine microplankton with sizes ranging from 20 to 200  $\mu\text{m}$  are abundant in such a stratified environment along with other meso-, macro-, and megaplanktonic organisms, which have  $Re$  in the range  $O(0.01\text{--}100)$  [35]. These observations insinuate the significant role of stratification in governing the locomotion of individual organisms as well as the interaction between two close organisms in the mentioned size range.

Much like inertia, stratification also significantly affects the motion of microswimmers. At low  $Re$ , the vertical migration of small organisms is hydrodynamically affected due to the rapid velocity decay as well as a higher energy expenditure in stratified fluids [36,37]. At a finite  $Re$ , stratification even leads to striking differences in the swimming speeds and stability of swimmers as compared to their motion in a homogeneous fluid [38]. The collective vertical migration of swimmers in a stratified fluid generates aggregation-scale eddies, which can potentially alter the physical and biogeochemical structure of the water column [32,39,40]. Stratification also leads to the accumulation of marine organisms such as plankton [41,42]. Thus, investigating the combined effects of inertia and stratification on the interaction between a pair of inter-

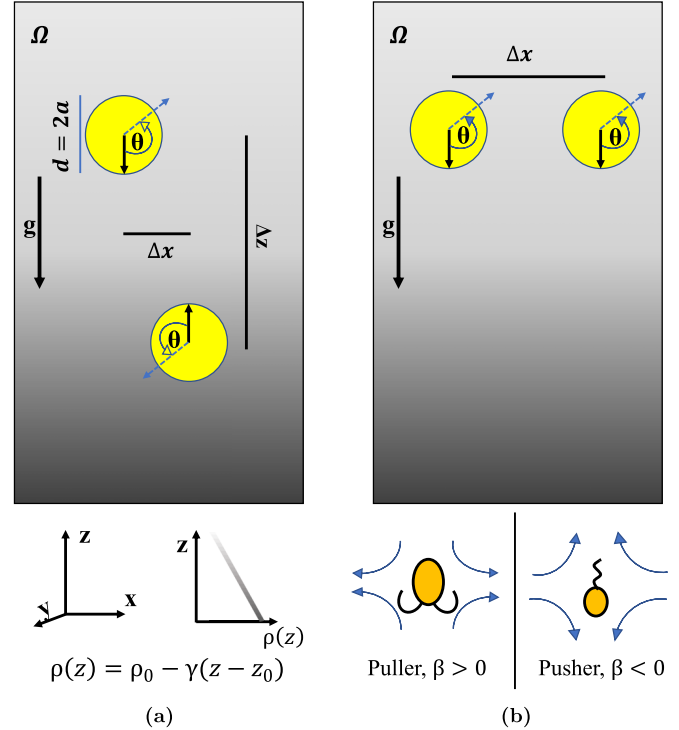


FIG. 1. Problem schematic. (a) Initial conditions for the pair of squirmers approaching each other in a linearly stratified fluid. (b) Initial conditions for a pair of squirmers moving side by side in a stratified fluid. The cartoons at the bottom in (b) show the flow fields generated by pullers ( $\beta > 0$ ) and pushers ( $\beta < 0$ ) as they move. The arrows in the squirmer bodies show their initial orientations. The darker shade of gray indicates higher density.

acting swimmers is a nontrivial and interesting problem that we address in this paper.

Looking at the interactions between a pair of organisms is crucial for modeling the collective dynamics of migrating marine organisms, e.g., swimmer schools in stratified environments. To this end, we numerically investigate the effect of density stratification on the interactions between a pair of inertial swimmers. We model the swimmers using the archetypal spherical squirmer model, which is explained in detail in Sec. II B. But first, we present the governing equations and the computational methodology used to solve these equations in Sec. II A. Then we discuss the findings of the simulations in Sec. III.

## II. GOVERNING EQUATIONS AND COMPUTATIONAL METHODOLOGY

We consider a pair of interacting squirmers moving through an incompressible Newtonian viscous fluid. The governing equations and the numerical procedure that is implemented to simulate the motion of a pair of interacting squirmers through a linearly stratified fluid at finite  $Re$  are presented in this section. We consider a linearly density stratified fluid such that the density increases in the downward  $z$  direction and the gravity is acting in the downward  $z$  direction, as shown in Fig. 1. The following sections explain the

governing equations and the numerical schemes used to solve them in detail.

### A. Flow and density fields

The fluid flow is governed by the Navier-Stokes equations for an incompressible Newtonian fluid and these equations are solved in the entire domain,  $\Omega$ . We simplify the Navier-Stokes equations for a fluid flow of a density stratified fluid using the Boussinesq approximation. The resulting equations can be written as

$$\rho_0 \frac{D\mathbf{u}}{Dt} = -\nabla P + \mu \nabla^2 \mathbf{u} + (\rho - \bar{\rho})\mathbf{g} + \mathbf{f}, \text{ in } \Omega, \quad (1)$$

$$\nabla \cdot \mathbf{u} = 0, \text{ in } \Omega, \quad (2)$$

where  $t$  is the time,  $\mathbf{u}$  is the velocity vector,  $P$  is the hydrodynamic pressure,  $\mathbf{g}$  is the acceleration due to gravity,  $\mu$  is the dynamic viscosity of the fluid,  $\rho_0$  is the reference fluid density, and  $\bar{\rho}$  is the volumetric average of the density over the entire domain.  $D(\cdot)/Dt$  is the material derivative.  $\rho$  is the local density at the grid point. We use the phase indicator function  $\psi$ , which is 1 inside the squirmer and 0 outside to mark the squirmer domain. The subscript  $f$  stands for fluid and  $s$  stands for squirmer.  $\mathbf{f}$  in Eq. (1) is the body force which accounts for fluid-solid interactions in the distributed Lagrange multiplier (DLM) method [43]. DLM has been widely used in the literature to simulate the motion of rigid particles and model swimmers in both homogeneous and stratified fluids [27,32,44–46].

The density field evolution is governed by the following advection-diffusion equation:

$$\frac{D\rho}{Dt} = \kappa \nabla^2 \rho, \text{ in } \Omega, \quad (3)$$

where  $\kappa$  is the diffusivity of the stratifying agent and  $\rho$  is the density field. We define Prandtl number  $\text{Pr} = \nu/\kappa$ , which is the ratio of the momentum diffusivity to the diffusivity of the stratifying agent. We split the density into two parts: (i) the initial linear background density profile  $\bar{\rho}(z)$  and (ii) the density perturbation induced by the motion of the squirmers,  $\rho'$ . So,

$$\rho = \bar{\rho}(z) + \rho'. \quad (4)$$

Here, the initial density of the fluid varies linearly with depth  $z$  as  $\bar{\rho}(z) = \rho_0 - \gamma(z - z_0)$ , where  $\gamma$  is the vertical density gradient and  $z_0$  is the location with reference density  $\rho_0$ . The stratification strength can be quantified by the Brunt-Väisälä frequency,  $N = (\gamma g/\rho_0)^{1/2}$ , the natural frequency of oscillation of a vertically displaced fluid parcel in a stratified fluid. By substituting Eq. (4) in Eq. (3), we obtain the following temporal and spatial evolution equation for the density perturbation  $\rho'$ :

$$\frac{D\rho'}{Dt} = -\mathbf{u} \cdot \nabla \bar{\rho}(z) + \kappa \nabla^2 \rho', \text{ in } \Omega. \quad (5)$$

We solve the advection-diffusion equation for the density perturbation  $\rho'$  and add it to the initial linear density profile to calculate the density field as shown in Eq. (4).

We use a finite volume method [47] to discretize Eqs. (1), (2), and (5) on a nonuniform staggered Cartesian fixed grid.

We use a second-order quasi-Crank-Nicolson method for the temporal evolution. Convection and diffusion terms in the momentum equation have been solved using quadratic upstream interpolation for convective kinetics (QUICK) and central-difference schemes [48], respectively. Both convection and diffusion terms in the density perturbation  $\rho'$  equation have been discretized using the central-difference scheme [32]. The numerical tool utilized for this study is based on the earlier version of PARIS [47]. We use periodic boundary conditions for velocity components and the density perturbation in all three directions.

### B. Swimmer model

Mathematically modeling the motion of a real microorganism is an enormously convoluted undertaking. This is due to the existence of a wide variety of length scales [roughly  $O(1)$ – $O(1000)$   $\mu\text{m}$  for common marine species], multitudes of swimming, grazing, and other behaviors depending on a range of parameters relating to their environments. In addition, these organisms exhibit a vast variety of shapes which might even not be the same, as individual microorganisms change their shape to feed, reproduce, or protect themselves from predators or hostile environments. Thus, we need to make several simplifications, even for the simplest microorganisms, in order to mathematically model and analyze them [22]. Hence, by necessity, we use a reduced-order squirmer model that is primitive. This model, however simple it may be, still includes important aspects of microorganism hydrodynamics, such as it swims and has a finite size so that excluded-volume effects and hydrodynamic interactions can be analyzed nontrivially.

The squirmer model [49,50] has been widely used as a model for swimmers such as *Volvox* in the literature [51]. In earlier studies, researchers utilized the squirmer model to investigate the motion of self-propelled organisms in a viscosity dominated flow regime, i.e.,  $\text{Re} \rightarrow 0$ . This allowed researchers to investigate various problems in a noninertial regime, such as the nutrient uptake by self-propelled organisms [52], hydrodynamic interactions between two squirmers [11], rheology of suspensions of squirmers [53], mixing by swimmers [54], as well as swimming in non-Newtonian fluids [55,56], using the squirmer model. Recently, researchers have studied the effect of finite inertia on the motion of swimmers by extending the squirmer model to low and intermediate Re number regimes [25–27,32,57,58]. The squirmer model was also used to study the effect of fluid density stratification on the motion of an individual squirmer [36,38] and the biogenic mixing induced by a swarm of swimming organisms [32] with low to intermediate Re. Thus, the squirmer model, owing to its simplicity and germane representation of the flow field generated by the self-propelling ciliary organisms, opens up a wide range of avenues for studying self-propulsion in various environmental conditions.

The squirmer self-propels by the wavelike motion of its surface. The spherical squirmer model, first introduced by Lighthill [49] and later modified by Blake [50], mimics the self-propulsion produced by the coordinated beating of a dense array of cilia on its surface. These axisymmetric ciliary deformations result in the radial ( $u_r^s$ ) and the tangential ( $u_\theta^s$ )

surface velocity components in a frame of reference attached to the squirmer with radius  $a$ :

$$u_r^s|_{r=a} = \sum_{n=0}^{\infty} A_n(t) P_n(\cos\theta), \quad (6)$$

$$u_\theta^s|_{r=a} = \sum_{n=1}^{\infty} \frac{-2}{n(n+1)} B_n(t) P_n^1(\cos\theta), \quad (7)$$

respectively. Here,  $r$  is the distance from the center of the squirmer,  $\theta$  is the angle measured from the direction of the locomotion,  $A_n$  and  $B_n$  are the time-dependent amplitudes of the ciliary deformations, and  $P_n, P_n^1$  are the associated Legendre polynomials of degree  $n$ . The swimming speed of a neutrally buoyant squirmer at  $\text{Re} = 0$ , i.e., in a Stokes flow, depends only on the first mode of each surface velocity component and is given by  $U_0 = (2B_1 - A_1)/3$ . This swimming speed is independent of fluid viscosity and other swimming modes [49].

For this study, we consider a reduced-order squirmer which has no radial velocity and only the first two modes of the surface tangential velocity,

$$u_\theta^s(\theta) = B_1 \sin\theta + B_2 \sin\theta \cos\theta, \quad (8)$$

where  $\theta$  is the angle with respect to the swimming direction, and  $B_1$  and  $B_2$  are the first two squirmering modes. The ratio  $\beta = B_2/B_1$  determines whether the squirmer is neutral ( $\beta = 0$ ), a puller ( $\beta > 0$ ), or a pusher ( $\beta < 0$ ). In the Stokes flow limit, the velocity of a squirmer in an unbounded domain is  $U_0 = 2B_1/3$ ; we use this as the velocity scale in this study. To impose the above given tangential velocity on the surface of the squirmer, we set the following divergence free velocity field inside the squirmer [57]:

$$\mathbf{u}_{in} = \left[ \left( \frac{r}{a} \right)^m - \left( \frac{r}{a} \right)^{m+1} \right] \left( u_\theta^s \cot\theta + \frac{du_\theta^s}{d\theta} \right) \mathbf{e}_r + \left[ (m+3) \left( \frac{r}{a} \right)^{m+1} - (m+2) \left( \frac{r}{a} \right)^m \right] u_\theta^s \mathbf{e}_\theta, \quad (9)$$

where  $a$  is the radius of the squirmer,  $r$  is the distance from the squirmer's center,  $\mathbf{e}_r$  and  $\mathbf{e}_\theta$  are the unit vectors in the radial and polar directions, and  $m$  is an arbitrary integer. The simulation results do not depend on the choice of  $m$ . The squirmer velocity is calculated by solving the following equations:

$$\mathbf{U} = \frac{1}{M_s} \int_{V_s} \rho_s (\mathbf{u} - \mathbf{u}_{in}) dV, \quad (10)$$

$$\mathbf{I}_s \cdot \boldsymbol{\omega} = \int_{V_s} \mathbf{r} \times \rho_s (\mathbf{u} - \mathbf{u}_{in}) dV, \quad (11)$$

where  $V_s$ ,  $M_s$ , and  $\mathbf{I}_s$  are the volume, mass, and the moment of inertia of the squirmer.  $\mathbf{U}$  and  $\boldsymbol{\omega}$  are the translational and the rotational velocities of the squirmer, respectively. Finally, the force  $\mathbf{f}$  is calculated by the following iterative formula:

$$\mathbf{f} = \mathbf{f}^* + \alpha \frac{\rho \psi}{\Delta t} (\mathbf{U} + \boldsymbol{\omega} \times \mathbf{r} + \mathbf{u}_{in} - \mathbf{u}), \quad (12)$$

where  $\mathbf{f}^*$  is the force calculated in the previous iteration and  $\alpha$  is a dimensionless factor chosen in such a way that iterations for calculating  $\mathbf{f}$  converge quickly [27,46]. Many organisms utilize techniques such as gas vesicles [59], carbohydrate

ballasting [60], and ion replacement [61,62] for buoyancy control. Hence, for this study, in order to isolate the effect of stratification on the motion of a squirmer, we consider the squirmer to be neutrally buoyant, i.e., the net buoyancy force acting on the squirmers due to differences in their density and the density of the fluid is zero at any instance of time. This is achieved by equating the density field inside the squirmer domain to the instantaneous background fluid density at that location  $[\rho_s(\mathbf{x}, t) = \bar{\rho}(\mathbf{x}) + \rho'(\mathbf{x}, t)]$ , where  $\mathbf{x}$  is any location inside the squirmer domain]. The same condition for neutral buoyancy was used for investigating the swimming dynamics of an individual squirmer with finite inertia in a stratified fluid [38]. In addition, we assume the  $\kappa$  to be uniform and the same for the squirmer and the background fluid [32,63].

### C. Simulation conditions

We explore the interactions of two squirmers moving towards each other leading to collision and two squirmers moving in the same direction side by side. We normalize the spatial parameters with the squirmer radius  $a$ , the velocities with  $U_0$ , and the time with the timescale  $a/U_0$ . We denote the dimensionless time with  $T$ .

The first case considered is that of a pair of squirmers approaching each other in opposite directions so that they collide. In this case, the squirmers are initialized at a center-to-center distance  $\Delta z$  and  $\Delta x$  in the  $z$  and  $x$  directions, respectively, in the  $y = 0$  plane. Their initial orientations are such that they are moving in opposite directions facing each other. We set  $\Delta z = 8$  and  $\Delta x = 1$ , unless stated otherwise [see Fig. 1(a)].

In the second case, where the squirmers are moving in the same direction side by side, we initialize them at the same initial vertical location  $z_i$ , separated by a center-to-center distance  $\Delta x$  in the  $x$  direction in the  $y = 0$  plane. We set  $\Delta x = 4$  unless mentioned otherwise [see Fig. 1(b)].

An earlier study in a homogeneous fluid considered only a colliding pair of squirmers in which the squirmers swim in the opposite direction [27]. We, however, consider colliding as well as side-by-side configuration, which covers squirmers moving opposite to each other as well as moving in the same direction. Also, the vertical direction is the preferred direction because, in many real-life situations, the swimmers move in the vertical direction such that they are parallel to the direction of the stratification or gravity mainly for grazing or in search of the sunlight during their diel cycles [64,65]. In addition, the direction of the motion considered in this study is one of the common situations for swimmers moving in oceans, e.g., bioconvection [66]. So, we initialize the squirmers with their initial orientations parallel to the direction of gravity, i.e., downwards or upwards.

When the squirmers approach very close to each other, the high pressure in the thin film between the squirmers prevents any nonphysical overlaps. However, a very small grid resolution is needed to resolve the thin liquid film and, consequently, it is computationally expensive. A repulsive force is imposed during the collision to prevent the nonphysical overlap [27,43],

$$\mathbf{F}_r = \frac{C_m}{\epsilon} \left( \frac{D - d - dr}{dr} \right)^2 \mathbf{n}, \quad (13)$$

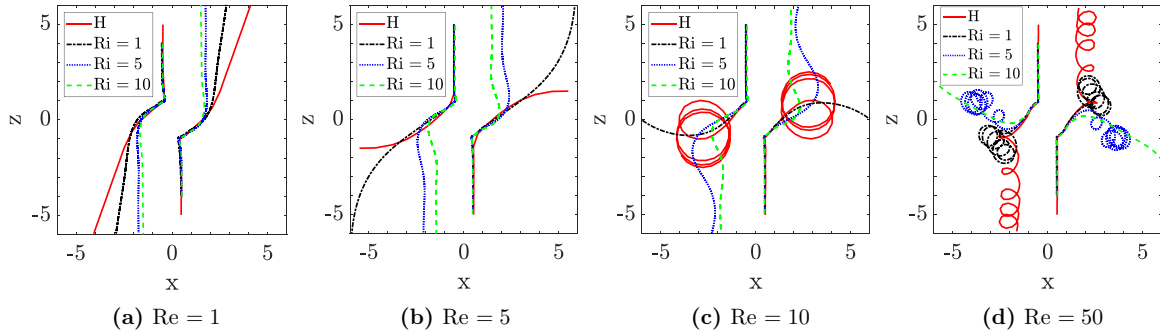


FIG. 2. Trajectories for colliding pullers with  $\beta = 5$  in a homogeneous and a stratified fluid with increasing stratification strengths. At low Re (1 and 5), stratification leads to reorientation of the pullers after their collision. For higher Re values (10 and 50), stratification results in the elimination of the close loop trajectories observed in a homogeneous fluid after the collision of two pullers.  $H$  in the legends stands for homogeneous fluid or  $Ri = 0$ .

where  $\epsilon = 10^{-4}$  is a small positive number,  $D$  is the distance between two squirmers,  $C_m = M_s U_0^2 / a$  is the characteristic force,  $d = 2a$  is the minimum possible distance, and  $dr$  is the force range and is set to be twice the smallest grid size  $\Delta$ . The direction of the repulsive force  $\mathbf{n}$  is along the squirmers' line of centers.

We carry out simulations for pushers and pullers with  $\beta = -5$  and  $5$ , respectively. The Re for the squirmers was varied between 1 and 50. To study the effects of stratification on the interaction of two inertial squirmers, we vary the Richardson number,  $Ri = \rho_0 a^3 N^2 / \mu U_0$ , which quantifies the relative importance of the buoyancy and the viscous forces, between 0 and 10. The domain size for this study is  $40a \times 20a \times 40a$  for the colliding squirmers case, while the domain size is  $40a \times 20a \times 80a$  for the side-by-side case. The smallest grid size was chosen such that there are around 35 grid points in one squirmer diameter, i.e.,  $\Delta \approx d/35$ . This grid size was found to be enough to resolve both the velocity and density boundary layers around the squirmers for the chosen Re range and  $Pr = 0.7$ . We present the grid independence tests in the Appendix.

It should be noted that we use  $Pr = 0.7$  for this study rather than  $Pr = 7$  or  $Pr = 700$ , which are the Pr values for a temperature stratified water and a salt stratified water, respectively. This has been done mainly to save the computational costs incurred by setting high values of Pr. In a stratified fluid, a density boundary layer is present in addition to the velocity boundary layer near the squirmer's surface. The thickness of this density boundary layer scales as  $\approx O(d/\sqrt{RePr})$ . For accurate resolution of the flow within this boundary layer, it is necessary to have at least a few grid points in it. This imposes limitations on the maximum mesh size that can be used for the simulations. Owing to the large size of the domain, using such a fine grid becomes computationally expensive. Hence, we use a smaller value for the Pr, which enables us to resolve the fluid flow as well as the density field in both the boundary layer and the outside. It has been shown in previous studies that changing the value of Pr merely changes the magnitudes of the velocities of the objects [46] and squirmers [38] moving in a stratified fluid, conserving the overall qualitative trends and behaviors. We discuss more on this in Sec. III E.

### III. RESULTS AND DISCUSSION

This section presents the important results from the simulations. We also present results on the interactions of a pair of inertial squirmers in a homogeneous fluid. The comparison between the trajectories of the squirmers and their velocities in the two distinct fluids allows us to investigate the effect of density stratification on the squirmer pair interactions.

#### A. Pairwise interactions of pullers in a stratified fluid

##### 1. Pullers approaching each other

Figure 2 shows the trajectories for two pullers approaching each other in opposite directions, initially oriented parallel to each other for  $Re = 1, 5, 10$ , and  $50$  in a homogeneous fluid and a stratified fluid with  $Ri = 1, 5$ , and  $10$ . In the absence of any density stratification, the trajectories of the colliding pullers reveal three patterns based on the magnitude of Re. At relatively low values of Re, i.e., 1 and 5, the pullers scatter away from each other with a positive scattering angle  $\phi$ , measured with respect to initial squirmer orientation. With increasing Re, i.e., from  $Re = 1$  to  $Re = 5$ ,  $\phi$  increases from  $\approx 20^\circ$  to a value just less than  $90^\circ$ . As we further increase the Re to a higher value of 10, the pullers do not escape each other after the collision but are trapped in clockwise loops with radii  $\approx 2a$ . At an even higher  $Re = 50$ , the pullers are no longer trapped and escape with  $\phi \approx 0^\circ$ , but keep on rotating in clockwise loops with diminished radii compared to the  $Re = 10$  case.

The introduction of stratification results in distinct changes in the trajectories of the interacting pullers, depending on their Re and the stratification strength, i.e., Ri. Stratification leads to a reduction in the scattering angle of the squirmers after the collision compared to their scattering angles in a homogeneous fluid, as can be seen in Figs. 2(a) and 2(b). For  $Re = 1$  [Fig. 2(a)], stratification reduces  $\phi$  from  $\approx 45^\circ$  in a homogeneous fluid to  $0^\circ$  for a stratified fluid with  $Ri = 10$ . For  $Re = 5$ ,  $\phi$  reduces to  $0^\circ$  for  $Ri = 10$  from  $\approx 90^\circ$  for a homogeneous fluid. Thus, at low inertia, high enough stratification leads to the reorientation of the pullers to their original orientation after the collision, unlike in a homogeneous fluid.

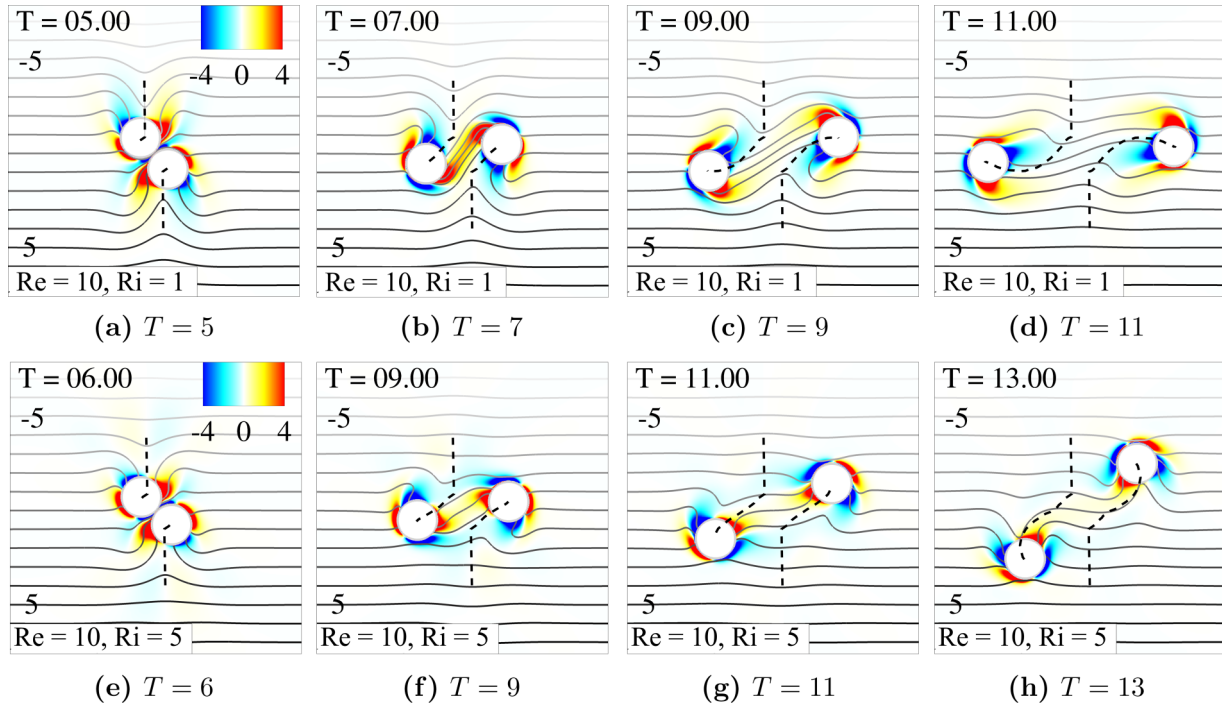


FIG. 3. Vorticity contours and isopycnals during the collision process of two approaching pullers with  $Re = 10$  at different stratification strengths, (a)–(d)  $Ri = 1$  and (e)–(h) 5. These plots show the interaction between the rear vorticity bubbles and the deformed isopycnals. The need of the displaced isopycnals to return to their original levels explain the rotational motion of the pullers after the collision. The isopycnals are the normalized density differences given by  $(\rho - \rho_0)/\gamma a$  and each line is one unit apart. The darker shade of the line color indicates a higher density value. The color bar for the vorticity contours is presented in the plots. The dashed lines show the trajectories of the pullers. These are snapshots of the flow field at different dimensionless times,  $T = tU_0/a$ , the value of which is indicated in the caption. The color bar is only shown in the first plot of each row for the neatness of the plots. For movies, see the Supplemental Material [67].

For higher  $Re = 10$ , stratification leads to the elimination of the rotating motion of the pullers in clockwise loops present in a homogeneous fluid [see Fig. 2(c)]. For  $Re = 10$ , pullers are no longer hydrodynamically trapped in the presence of density stratification, unlike in the homogeneous fluid. They scatter away from each other with a positive scattering angle, much like lower  $Re$  cases, which decreases with an increase in the stratification strength. Again, high enough stratification strength leads to the reorientation of the pullers to their original orientation [see Fig. 2(c)]. For  $Re = 50$ , only a high stratification results in the elimination of the clockwise loops in the trajectories of the pullers after the collision. This is clear from the trajectories of pullers with  $Re = 50$  in a stratified fluid with  $Ri = 10$  [Fig. 2(d)]. The pullers escape from each other, but with a large scattering angle which is greater than  $90^\circ$ . However, a lower stratification ( $Ri = 1$  and 5) leads to the hydrodynamic trapping of the pullers after the collision in this case, which is similar to the  $Re = 10$  case in a homogeneous fluid.

To explain the reorientation of the pullers after the collision, the elimination of the closed loop trajectories, and the prevention of the hydrodynamic trapping of the pullers, we plot the vorticity contours and isopycnals at different time instances during the collision process of the pullers for two stratification strengths in Fig. 3. The effect of increasing the inertia (or  $Re$ ) of pullers is to increase the size of the vorticity bubble in the rear part of their bodies [26]. The introduction

of stratification reduces the size of these recirculatory regions behind pullers [38]. The trapping of the pullers in loops after the collision in a homogeneous fluid can be explained by the interaction between the bigger recirculatory regions behind the pullers at higher  $Re = 10$  and 50 [27]. Since stratification leads to shrinking in the size of these rear recirculatory regions, the interaction between these rear bubbles is limited at finite  $Ri$  values. This prevents the pullers from attaining a constant angular velocity after the collision, unlike the homogeneous case [see Fig. 4(b)]. This damping of the angular velocity of the pullers after the collision essentially allows the pullers to scatter away from each other without being trapped in counterclockwise loops. This point becomes clear in Fig. 3, where we plot the vorticity contours and isopycnals for  $Re = 10$  in stratified fluids with different stratification strengths,  $Ri = 1$  and  $Ri = 5$ , respectively.

As the pullers move down (up) in a stratified fluid, they trap lighter (heavier) fluid in their rear recirculatory bubbles, which can be seen in terms of deformed isopycnals in Fig. 3. After the collision, the axisymmetry of the flow and the isopycnal deformations are broken. The interaction between the rear vorticity bubbles rotates the pullers in a clockwise direction, as can be seen in Fig. 3(b). However, the tendency of the deformed isopycnals behind the pullers to return to their original positions reduces the effect of this interaction on the puller orientations [Fig. 3(f)]. The counterclockwise torque due to the flow induced by the need of the deformed

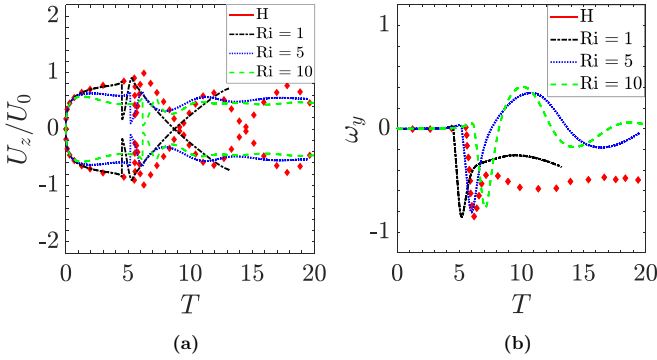


FIG. 4. Time evolution of the (a) translational velocity and (b) rotational velocity of two approaching pullers during the collision process at different  $Ri$  values for a fixed  $Re = 10$ . Stratification eliminates the oscillations in the translational velocity and prevents the pullers from attaining a constant angular velocity, thus eliminating the closed loop trajectories as observed in the case of a homogeneous fluid. Stratification also results in a change in the sign of the angular velocity, which reorients the pullers in their original orientations after the collision at high enough  $Ri$ .

isopycnals to return to their original positions determines the rotational motion of the pullers after the collision and leads to the reorientation of the pullers in the original orientation. This prevents them from getting trapped into loops. This is clear from the comparison of the isopycnal deformation in Figs. 3(c) and 3(g).

At high  $Ri$ , i.e.,  $Ri = 5$  as compared to  $Ri = 1$ , the isopycnals are less deformed, indicating that the resistance to the displacement of the isopycnals due to the flow induced by the squirmers is stronger. This prevents the clockwise rotation of the pullers and reorients them. Thus, the competition between the rear vorticity bubble interactions and the tendency of deformed isopycnals to return to their original levels determines the rotational motions and the orientations of the pullers after the collision. Owing to the smaller size of the rear vorticity bubbles of pullers in a stratified fluid compared to a homogeneous fluid [38], the effect of the stratification dominates the vorticity bubble interactions between the two pullers at high  $Ri$  values. This prevents the pullers from attaining a constant angular velocity, unlike in a homogeneous fluid, and thus eliminates the closed loops for  $Re = 10, 50$  and results in the reorientation of the pullers for  $Re = 1, 5$ , and  $10$ .

The consequences of the mentioned vorticity and isopycnal interactions on the colliding pullers can be understood from their translational and angular velocities. Velocity evolution for two approaching pullers is plotted in Fig. 4 for  $Re = 10$  and various stratification strengths. Stratification leads to the elimination of the oscillations in the translational velocities of the pullers after the collision and allows them to attain a steady velocity, which results in their escape from each other [Fig. 4(a)]. In addition, the tendency of the displaced isopycnals to return to their neutrally buoyant levels prevents the pullers from attaining a constant angular velocity as can be seen in Fig. 4(b). This results in the reorientation of the pullers to their original orientation.

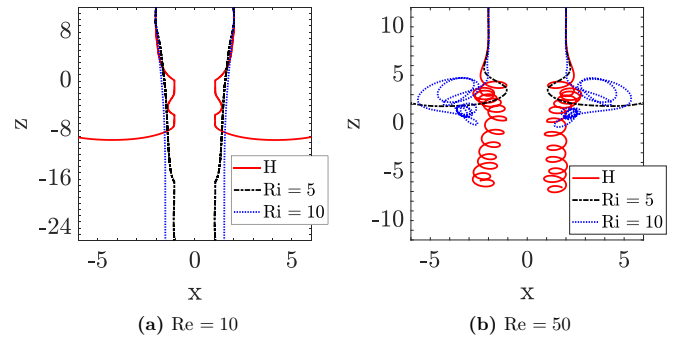


FIG. 5. Trajectories of a pair of pullers,  $\beta = 5$ , moving side by side initially separated by a distance  $4a$  in the  $x$  direction at various stratification strengths. (a)  $Re = 10$ , (b)  $Re = 50$ .  $H$  in the legends stands for homogeneous fluid or  $Ri = 0$ .

## 2. Pullers moving side by side

In addition to squirmers approaching each other in opposite directions and colliding, we also investigate the motion of a pair of squirmers moving side by side initially apart by  $\Delta x$  in the  $x$  direction. Figure 5 shows the trajectories of two pullers moving side by side in different stratification strengths at  $Re = 10$  and  $50$ . In a homogeneous fluid, pullers moving side by side exhibit completely separate trajectories at  $Re = 10$  and  $Re = 50$ . At  $Re = 10$ , the pullers are initially attracted towards each other and they come close and stick together while they move downward. They move away from each other but are pulled together after a while. They again move down together a little before being repelled away from each other and, finally, scatter away in the horizontal direction [see Fig. 5(a)]. For  $Re = 50$ , the pullers are slightly repelled from each other initially. But they are pulled towards each other, which also leads to a torque on them, making them rotate in a loop while they move down [see Fig. 5(b)]. Thus, in a homogeneous fluid, a pair of pullers moving side by side scatter away from each other at  $Re = 10$ , while they are hydrodynamically trapped near each other in loops for  $Re = 50$ .

The introduction of stratification increases the attraction between the pullers moving side by side at  $Re = 10$  [see Fig. 5(a)]. At  $Ri = 5$  and  $10$ , this increase in the attraction between the pullers increases the time that the pullers spend near each other before they collide and prevents the pullers from separating unlike in a homogeneous fluid. As a result, once the pullers collide sideways, they stick together and move further down.

The significant changes in the trajectories of two pullers moving side by side due to stratification can also be seen at a higher  $Re$  ( $=50$ ); see Fig. 5(b). For  $Ri = 5$ , the pullers are again hydrodynamically trapped near each other in loops, but they do not move much in the downward direction. Increasing the stratification further to  $Ri = 10$ , the pullers are attracted towards each other, leading to a sideways collision. However, after this collision, they repel away from each other and scatter in the horizontal direction, similar to what happens eventually for  $Re = 10$  in a homogeneous fluid. This is expected as stratification leads to a reduction in the squirmer velocities. This reduces their effective  $Re$ , which explains the qualitative

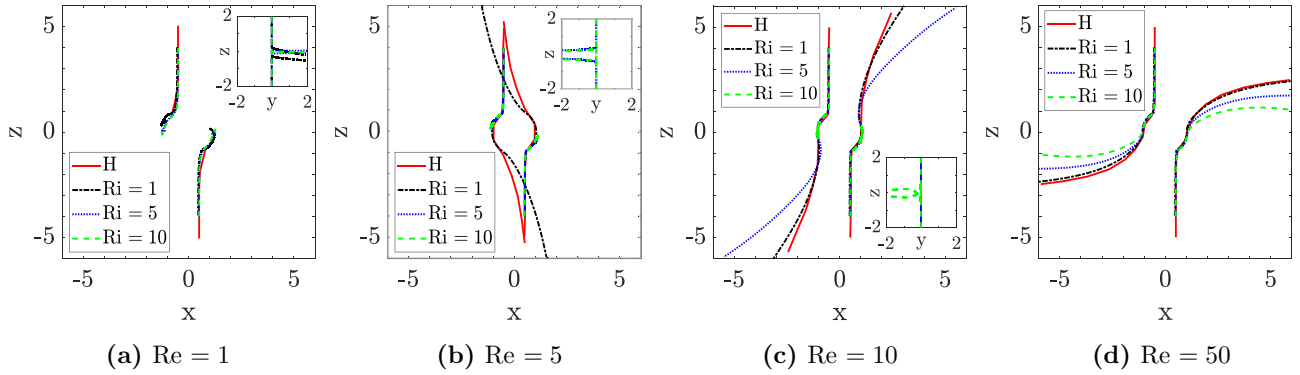


FIG. 6. Trajectories for colliding pushers with  $\beta = -5$  in a homogeneous and a stratified fluid with increasing stratification strengths. At low  $Re = 1, 5$ , and  $10$ , high enough stratification leads to the stoppage of the pushers as they collide. This state is not stable and, as a result, the pushers are deflected away from the  $xz$  plane in the  $y$  direction. The pushers stick together as they move in the  $y$  direction after the deflection, indicating that stratification leads to hydrodynamic trapping of colliding pushers. This deflection away from the  $xz$  plane is shown in the insets in (a)–(c). This instability is gradually prevented with increasing  $Re$  and the pushers no longer stop or are deflected at high  $Re$ , i.e.,  $Re = 50$ .  $H$  in the legends stands for homogeneous fluid.

similarities between the trajectories in the high  $Re$ –high  $Ri$  and the low  $Re$ –no stratification cases.

## B. Pairwise interactions of pushers in a stratified fluid

### 1. Pushers approaching each other

Figure 6 shows the trajectories for two pushers approaching each other in opposite directions, initially oriented parallel to each other for  $Re = 1, 5, 10$ , and  $50$  in a homogeneous fluid and a stratified fluid with different  $Ri$ . In the absence of any density stratification, the trajectories of the colliding pushers reveal two patterns based on the magnitude of  $Re$ . At relatively low values of  $Re$ , i.e.,  $1$ , the pushers come to a complete stop after the collision. However, this configuration is unstable and the pushers are deflected away from the  $y = 0$  plane, resulting in a three-dimensional (3D) motion after the collision [27]. This behavior is common for interacting pushers for  $Re \ll 1$  and is due to the instability in their two-dimensional (2D) motion once they come close to each other [14]. As we increase the  $Re$  further, the pushers escape each other after the collision with a scattering angle  $\phi < 90^\circ$ .  $\phi$  increases with an increase in the inertia of the pushers, with values  $\approx 0^\circ$ ,  $\approx 30^\circ$ , and  $\approx 90^\circ$  for  $Re = 5, 10$ , and  $50$ , respectively.

The introduction of stratification results in distinct changes in the trajectories of the interacting squirmers, depending on their  $Re$  and the stratification strength, i.e.,  $Ri$ . At low  $Re$ , the effect of introducing stratification on the trajectories of colliding pushers is to trap them near each other by bringing them to a complete stop. However, these states are not stable and soon the pushers leave the plane of collision, i.e., the  $xz$  plane, and are deflected in the  $y$  direction. The pushers stick together as they leave the  $y = 0$  plane and continue to move together in the  $y$  direction, as shown in the insets of Figs. 6(a) and 6(b). The same is true for a high enough stratification at higher  $Re$ . The pushers come to a standstill after the collision and move together in the  $y$  plane for  $Re = 10$  at  $Ri = 10$ . Introduction of the stratification leads to the reduction in the translational velocities of the pushers, which reduces their effective inertia, resulting in low  $Re$  like trajectories even at high  $Re$  values.

For intermediate  $Re = 10$  and high  $Re = 50$ , the effect of stratification depends on the magnitude of  $Ri$ . The trapping due to the stoppage of the pushers after their collision at low  $Re$  values and the 3D trajectories are progressively prevented at high  $Re$  values. This can be seen in Figs. 6(c) and 6(d). At high  $Re$  and low  $Ri$ , the effect of inertia is significant compared to the effect of stratification. As a result, the pushers try to move away from each other, similar to what happens in a homogeneous fluid. This can be observed for  $Re = 10$  at  $Ri = 1$  and  $5$ , and  $Re = 50$  at  $Ri = 1, 5$ , and  $10$  for which pushers are scattered away from each other with  $\phi \approx 45^\circ$  and  $90^\circ$ , respectively.

We plot the vorticity contours and the isopycnals in Fig. 7 for  $Re = 10$  at two  $Ri$  values, viz.,  $1$  and  $5$ . The interaction of the pushers with the isopycnals reveals the reason behind the deflection from their trajectories in a homogeneous fluid for high  $Re$  values ( $10$  and  $50$ ). Figure 7 shows that as the pushers move forward, they displace the isopycnals behind them owing to the long vorticity trail behind them. However, as  $Ri$  increases, these displaced isopycnals resist the flow induced by the pushers as they try to return to their original levels. The strength of opposition by the displaced isopycnals to their further deformation increases with  $Ri$ . For example, for  $Ri = 1$  [Figs. 7(a)–7(d)], the isopycnals behind the pushers are deformed for a longer time, while they return to their original levels quickly for  $Ri = 5$  [Figs. 7(e)–7(h)]. As a result of the interaction between the rear vorticity bubbles and the deformed isopycnals in the wake of the pushers, their  $y$  angular velocity increases [see Fig. 8(b)] and the pushers are deflected to their right.

Figure 8 shows the translational and rotational velocities of the pushers at various stratification strengths for  $Re = 10$ . It can be seen from Fig. 8(a) that the translational velocities of the squirmers decrease with increasing stratification, both before and after the collision. The reason for this decrease is the trapping of lighter (heavier) fluid in the recirculatory region, which in the front region leads to a higher buoyancy force on them as they move in a heavier (lighter) fluid. For a high enough  $Ri$  value (e.g.,  $Ri = 10$  at  $Re = 10$ ), the velocity reduction is large enough to lead to instability,



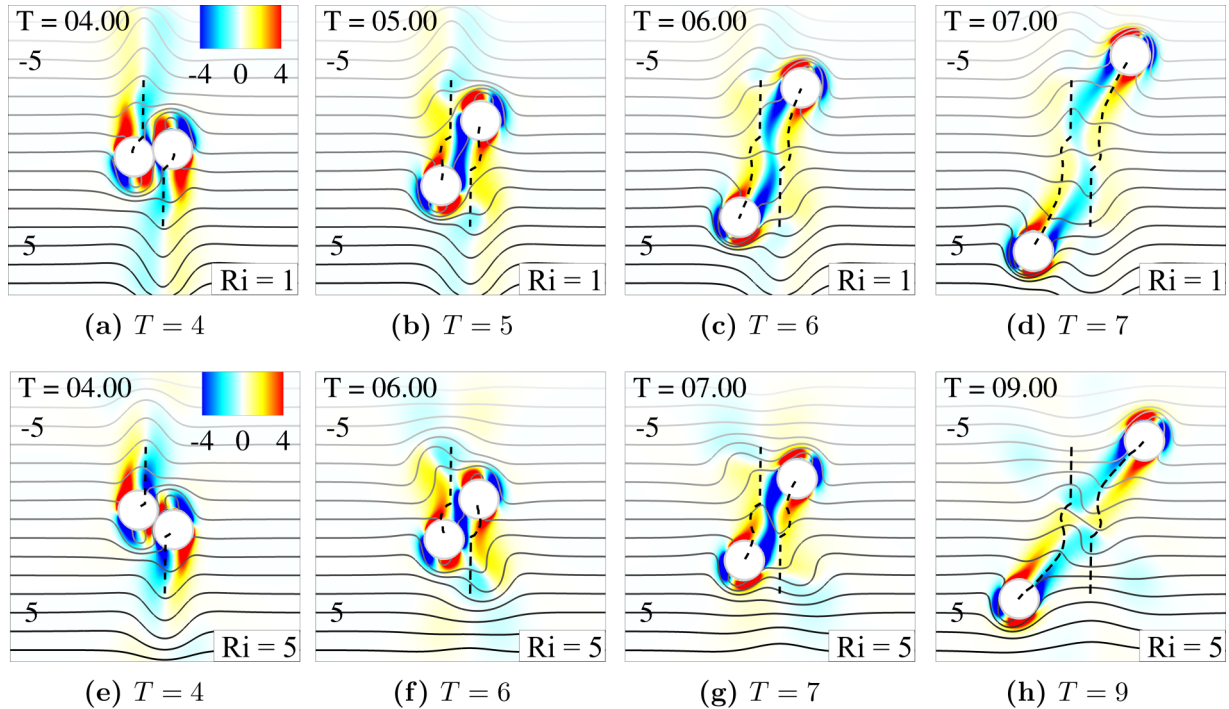


FIG. 7. Vorticity contours and isopycnals during the collision process of two approaching pushers with  $Re = 10$  at different stratification strengths, (a)–(d)  $Ri = 1$  and (e)–(h) 5. These plots show the interaction between the vorticity bubbles and the deformed isopycnals. The need of the displaced isopycnals to return to their original levels determine the trajectories of the pushers after the collision. The isopycnals are the normalized density differences given by  $(\rho - \rho_0)/\gamma a$  and each line is one unit apart. The darker shade of the line color indicates a higher density value. The color bar for the vorticity contours is presented in the plots. Dashed lines indicate the pusher trajectories. These are snapshots of the flow field at different dimensionless times,  $T = tU_0/a$ , the value of which is indicated in the caption. The color bar is only shown in the first plot of each row for the neatness of the plots. For movies, see the Supplemental Material [67].

which deflects them away from the  $y = 0$  plane. For the cases when the collision process does not lead to an instability (e.g.,  $Ri = 1$  and 5 at  $Re = 10$ ), stratification increases the magnitude of the rotational velocity of the pushers, which causes the

divergence in their trajectories after the collision compared to their homogeneous fluid trajectories [see Fig. 8(b)].

2. Pushers moving side by side

In contrast to a pair of pullers moving side by side, stratification has a limited effect on the trajectories of a pair of pushers moving side by side, which is shown in Fig. 9. For all the explored  $Re$  values, i.e., 10 and 50, the pushers

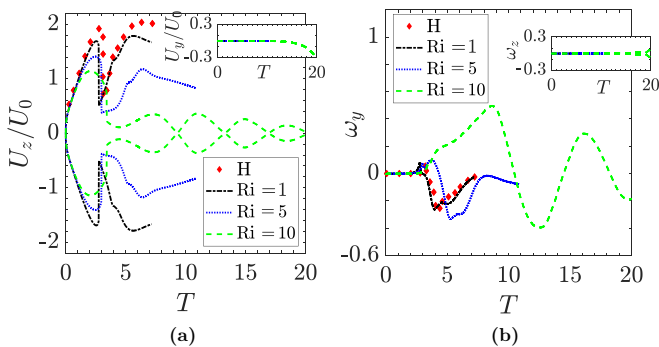


FIG. 8. Time evolution of the (a) translational velocity and (b) rotational velocity of two approaching pushers during the collision process at different  $Ri$  values for a fixed  $Re = 10$ . Stratification leads to a significant reduction in the velocities of the pushers after their collision. At a high stratification, the pushers almost come to a stop after the collision and eventually are deflected away from the  $y = 0$  plane, which is shown by the time evolution of the  $y$  velocities of the pullers in the insets.

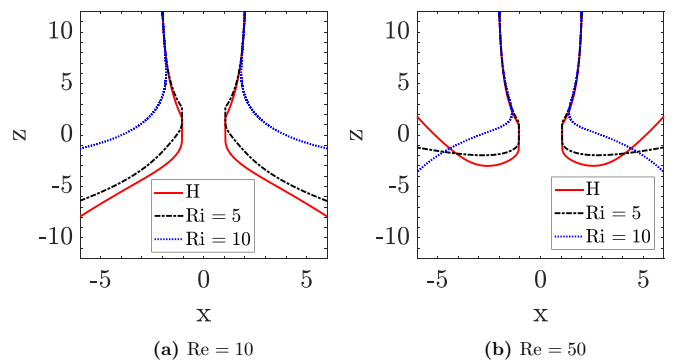


FIG. 9. Trajectories of a pair of pushers,  $\beta = -5$ , moving side by side initially separated by a distance  $4a$  in the  $x$  direction at various stratification strengths. (a)  $Re = 10$ , (b)  $Re = 50$ .  $H$  in the legends stands for homogeneous fluid or  $Ri = 0$ .

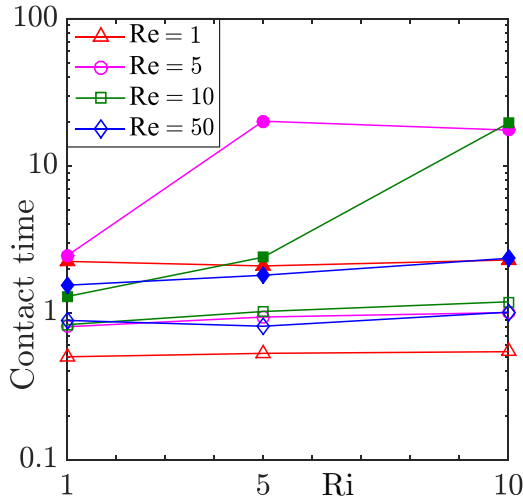


FIG. 10. Contact time, i.e., time spent by the squirmers near (center-to-center distance  $\leq 2.12$ ) each other for colliding squirmer pairs. Hollow symbols are for pullers and filled symbols are for pushers.

are initially attracted towards each other. But this attraction does not last very long and eventually they deflect away from each other. The effect of stratification is to lower the  $z$  value where the pushers first start to separate from each other. Here we measure the scattering angle as the angle that the final pusher orientation makes with its initial orientation.

In a homogeneous fluid, the pushers are attracted to each other at  $Re = 10$  and  $50$ . As they come very close, they stick together and move down before deflecting away. Increasing the inertia of the pushers leads to an increase in their scattering angle after the deflection (see Fig. 9). Increasing the stratification strength hastens the process of repulsion, leading to the pushers being pushed away at lower  $z$  distances from their initial positions as compared to a homogeneous fluid. At a high stratification, the pushers are pushed away from each other even before they can come very close to each other, as they do in a homogeneous fluid. This is observed from the pusher trajectories at  $Ri = 10$  for both  $Re$  values in Fig. 9. In addition, at  $Re = 50$ , increasing the stratification leads to a reduction in the scattering angles of the pushers. However, at  $Re = 10$ , stratification results in a slight increase in the scattering angles of the pushers. Again, there are qualitative similarities in the trajectories of the pushers at high  $Re$ -high  $Ri$  and low  $Re$ -no stratification values, as we observed in the case of a pair of pullers, which is due to the reduction in the effective  $Re$  of the pushers at high  $Ri$  due to the reduction in their swimming speeds.

### C. Contact time

Figure 10 plots the contact time for a pair of squirmers colliding with each other against  $Ri$  for various  $Re$  values explored in this study. We define contact time as the time spent by the squirmers in contact, i.e., when their center-to-center distance is less than  $d + 2\Delta$ , which is also the distance when the repulsive force between the squirmers is active. For

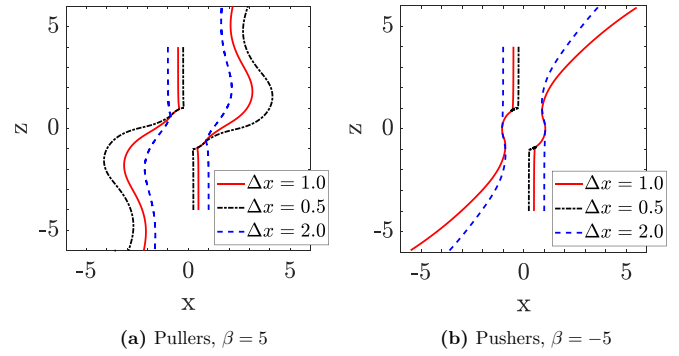


FIG. 11. Trajectories of a pair of colliding (a) pullers,  $\beta = 5$ , and (b) pushers,  $\beta = -5$ , for different  $\Delta x$ .  $Re = 10$  and  $Ri = 5$ .

the cases where the squirmers deflect away from the  $y = 0$  plane, we measure contact time just before the squirmers are deflected. We observe that pushers spend more time in contact as compared to pullers for the range of parameters explored in this study. The contact time increases slightly with  $Ri$  for all the cases except for pushers with  $Re = 5$  and  $10$ . This is because the pushers are separated from each other at low  $Ri$ , while they are trapped and deflect in the third direction at high  $Ri$  for  $Re = 5$  and  $10$ .

In many real-life situations, it is beneficial to estimate the contact time of swimmers. For reproductive purposes, it is beneficial for the swimmers to spend more time in contact, while they do not want to be in contact with a predator and escape as soon as possible. The results thus can be used to predict the encounter time of pusher and puller swimmers to predict their success in reproduction and feeding or escaping from predators. These results show that pushers tend to spend more time in contact than pullers, which increases with increasing the stratification. This can enhance their success in reproduction in stratified environments.

### D. Effect of initial lateral spacing

Figure 11 shows the effect of changing  $\Delta x$  on the trajectories of a pair of colliding squirmers for  $Re = 10$  and  $Ri = 5$ . These results show that changing  $\Delta x$  for pullers does not change the trajectories of the pullers significantly, as they are qualitatively the same. However,  $\Delta x$  has a significant role in determining the trajectories of colliding pushers. For  $\Delta x = 1$  and  $2$ , the pushers collide and separate from each other, while for a smaller  $\Delta x (=0.25)$ , the pushers stop after the collision, which is similar to what happens for high stratification at larger  $\Delta x$ . Thus, decreasing  $\Delta x$  simply decreases the  $Ri$  above which the instability in the colliding squirmer configuration sets in. Thus, the details of the trajectories are more closely related to the initial configuration for pushers than for pullers.

### E. Effect of Prandtl number

In this section, we briefly discuss the effects of varying  $Pr$  on the trajectories of a colliding pair of pullers and pushers. We assumed  $Pr = 0.7$  for this study in order to resolve the density boundary layer; but for temperature stratified water,

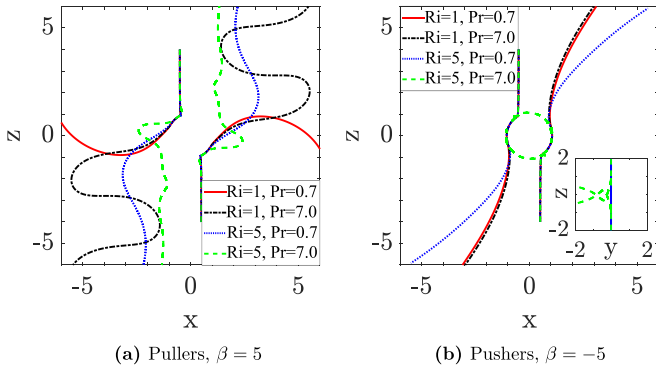


FIG. 12. Trajectories of a pair of pushers,  $\beta = -5$ , moving side by side initially separated by a distance  $4a$  in the  $x$  direction at various stratification strengths. (a)  $Re = 10$ , (b)  $Re = 50$ .  $H$  in the legends stands for homogeneous fluid or  $Ri = 0$ .

$Pr = 7$ , while  $Pr = 700$  for salt stratified water. Resolving the density boundary layer [ $\approx O(d/\sqrt{RePr})$ ] becomes computationally expensive with increasing  $Pr$ . Hence a small value of  $Pr$  was used to save the computational penalty. Changing  $Pr$  of the fluid quantitatively changes the settling velocity of a rigid sphere [46] and the swimming velocity of neutrally buoyant squirmers [38], while the qualitative trend remains the same in both of these cases. Thus, changing  $Pr$  will also change the trajectories of a pair of squirmers interacting in a stratified fluid. In addition, the transition from one type of trajectory to the other will happen at different values of  $Re$  and  $Ri$ .

We present the trajectories of a pair of pullers and pushers colliding for two different  $Ri$  and  $Pr$  in Fig. 12. For a pair of colliding pullers with  $Re = 10$ , the pullers swim away from each other even at  $Pr = 7$ ; however, their trajectories are different compared to the  $Pr = 0.7$  case. On the other hand, for pushers, the trajectories are similar for a lower  $Ri$ . But the swimmers get trapped near each other for  $Ri = 5$  in the case of  $Pr = 7$ , unlike the case when  $Pr = 0.7$ . These results show that the details of the trajectories, i.e.,  $Ri$  for which they have separate, exact trajectories and  $Ri$  for which they get trapped near each other and deflect away from the initial plane, depend on the value of  $Pr$ . This is expected as  $Pr$  governs the size of the density boundary layer, which has an important role in determining the near-field interactions between swimmers.

IV. CONCLUSIONS

We investigate the interactions of a pair of squirmers with finite inertia in a stratified fluid with different stratification strength. We compare the squirmer trajectories and velocities with their trajectories and velocities in a homogeneous fluid for the same initial conditions. We present results for two types of initial configurations: (1) squirmers approaching each other in opposite directions, and (2) squirmers moving side by side in the vertical direction. The presented results are potentially important in understanding the collective dynamics of microorganisms in oceans and lakes where stratification is observed.

For a pair of pullers approaching each other, stratification leads to their reorientation after the collision, contrary to what

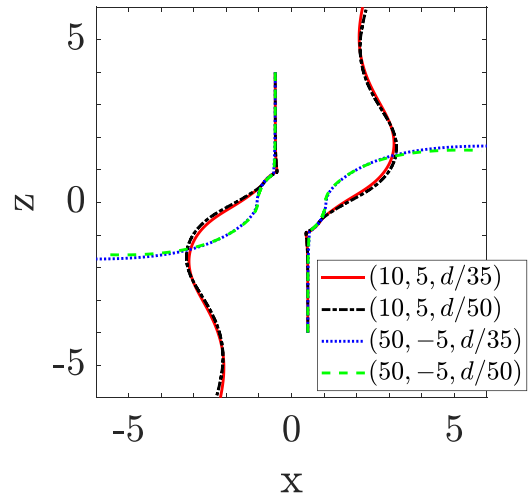


FIG. 13. Trajectories of a pair of colliding squirmers at two different grid resolutions. Legends are for  $(Re, \beta, \Delta)$ . Here,  $Ri = 5$  for all cases.

happens in a homogeneous fluid. The tendency of the displaced isopycnals behind the pullers results in a torque on the pullers which reorients the pullers in their initial orientation after the collision. Stratification also leads to the elimination of the closed loop trajectories observed for colliding pullers at high  $Re$  ( $=10$  and  $50$ ), which has been explained using the flow field and the density field around the pullers during and after the collision.

A pair of pullers moving side by side follow complicated and distinct trajectories at different  $Re$  and  $Ri$ . In a homogeneous fluid, the pullers are repelled away from each other after initial attraction and a close contact for  $Re = 10$ , but they are hydrodynamically trapped near each other in loops as they move down for  $Re = 50$ . Again, high stratification leads to the elimination of the loops and hydrodynamic trapping deflecting the pullers away from each other even at  $Re = 50$ , similar to what happens for  $Re = 10$  pullers in a homogeneous fluid.

A pair of pushers come to a complete stop after the collision at high  $Ri$ . However, this configuration is unstable, which results in a 3D motion of the pushers away from the plane of collision. As the pushers move away from the plane of collision, they stick together. The 3D motion is gradually prevented as we increase  $Re$ , and a higher  $Ri$  is required for the instability. These results indicate that in a stratified fluid, organisms might get trapped near each other and move horizontally, which can lead to their accumulation in oceans [41,42].

In a homogeneous fluid, two pushers moving side by side are attracted towards each other, but eventually, they scatter away from each other with a scattering angle increasing with  $Re$ . Stratification hastens the repulsion between the pullers moving side by side and results in a decrease in the scattering angle at high  $Re$ .

The results for contact time for the squirmers show that pushers tend to spend more time in contact with each other than pullers. Furthermore, stratification increases the contact time for the squirmers. This indicates an enhanced chance for their success in reproduction in stratified environments. We

also present results for variation in the Pr of the fluid and different lateral initial separations of the squirmers. But these were limited to a few cases to save computational expenses. Logical extensions of this work are to study the effects of varying the fluid Pr, the effects of squirmer swimming mode  $\beta$ , the effects of initial squirmer configurations, and the effects of buoyancy by relaxing the quasi-instantaneous neutral buoyancy condition on the interactions of squirmers in a stratified fluid.

#### ACKNOWLEDGMENTS

The authors would like to acknowledge financial support from the National Science Foundation via Grants No. CBET-1604423, No. CBET-1700961, and No. CBET-1705371. This work used the Extreme Science and Engineering Discovery

Environment (XSEDE) [68], which is supported by the National Science Foundation Grant No. ACI-1548562 through allocations TG-CTS180066 and TG-CTS190041.

#### APPENDIX: GRID AND DOMAIN INDEPENDENCE

We present the grid independence test results in this Appendix. Figure 13 shows the trajectories for a pair of squirmers approaching each other in opposite directions for two different grid sizes. As can be seen in the figure, changing the grid size from  $\Delta = d/35$  to  $\Delta = d/50$  results in a negligible variation in the trajectories of the colliding squirmers. Here,  $\Delta$  is the smallest grid size. Hence, to save the computational cost, we carried out all the simulations with  $\Delta = d/35$ . Further validations for the homogeneous fluid cases can be found in Ref. [27].

- [1] C. Dombrowski, L. Cisneros, S. Chatkaew, R. E. Goldstein, and J. O. Kessler, Self-Concentration and Large-Scale Coherence in Bacterial Dynamics, *Phys. Rev. Lett.* **93**, 098103 (2004).
- [2] H. H. Wensink, J. Dunkel, S. Heidenreich, K. Drescher, R. E. Goldstein, H. Löwen, and J. M. Yeomans, Meso-scale turbulence in living fluids, *Proc. Natl. Acad. Sci.* **109**, 14308 (2012).
- [3] A. Sokolov, I. S. Aranson, J. O. Kessler, and R. E. Goldstein, Concentration Dependence of the Collective Dynamics of Swimming Bacteria, *Phys. Rev. Lett.* **98**, 158102 (2007).
- [4] X.-L. Wu and A. Libchaber, Particle Diffusion in a Quasi-Two-Dimensional Bacterial Bath, *Phys. Rev. Lett.* **84**, 3017 (2000).
- [5] F. E. Fish, Kinematics of ducklings swimming in formation: Consequences of position, *J. Expt. Zool.* **273**, 1 (1995).
- [6] B. S. Beckett, *Biology: A Modern Introduction* (Oxford University Press, New York, 1986).
- [7] D. Saintillan and M. J. Shelley, Orientational Order and Instabilities in Suspensions of Self-Locomoting Rods, *Phys. Rev. Lett.* **99**, 058102 (2007).
- [8] E. Lushi, H. Wioland, and R. E. Goldstein, Fluid flows created by swimming bacteria drive self-organization in confined suspensions, *Proc. Natl. Acad. Sci.* **111**, 9733 (2014).
- [9] A. T. Chwang and T. Y.-T. Wu, Hydromechanics of low-Reynolds-number flow. Part 2. Singularity method for Stokes flows, *J. Fluid Mech.* **67**, 787 (1975).
- [10] K. Drescher, K. C. Leptos, I. Tuval, T. Ishikawa, T. J. Pedley, and R. E. Goldstein, Dancing Volvox: Hydrodynamic Bound States of Swimming Algae, *Phys. Rev. Lett.* **102**, 168101 (2009).
- [11] T. Ishikawa and M. Hota, Interaction of two swimming paramecia, *J. Expt. Biol.* **209**, 4452 (2006).
- [12] X. Chen, X. Yang, M. Yang, and H. Zhang, Dynamic clustering in suspension of motile bacteria, *Europhys. Lett.* **111**, 54002 (2015).
- [13] A. P. Petroff, X.-L. Wu, and A. Libchaber, Fast-Moving Bacteria Self-Organize into Active Two-Dimensional Crystals of Rotating Cells, *Phys. Rev. Lett.* **114**, 158102 (2015).
- [14] T. Ishikawa, M. Simmonds, and T. J. Pedley, Hydrodynamic interaction of two swimming model microorganisms, *J. Fluid Mech.* **568**, 119 (2006).
- [15] I. O. Götze and G. Gompper, Mesoscale simulations of hydrodynamic squirmer interactions, *Phys. Rev. E* **82**, 041921 (2010).
- [16] T. Ishikawa, G. Sekiya, Y. Imai, and T. Yamaguchi, Hydrodynamic interactions between two swimming bacteria, *Biophys. J.* **93**, 2217 (2007).
- [17] G. P. Alexander, C. M. Pooley, and J. M. Yeomans, Scattering of low-Reynolds-number swimmers, *Phys. Rev. E* **78**, 045302(R) (2008).
- [18] A. Furukawa, D. Marenduzzo, and M. E. Cates, Activity-induced clustering in model dumbbell swimmers: The role of hydrodynamic interactions, *Phys. Rev. E* **90**, 022303 (2014).
- [19] R. Maniyeri and S. Kang, Hydrodynamic interaction between two swimming bacterial flagella in a viscous fluid—A numerical study using an immersed boundary method, *Prog. Comput. Fluid Dynam.* **14**, 375 (2014).
- [20] C. M. Pooley, G. P. Alexander, and J. M. Yeomans, Hydrodynamic Interaction between Two Swimmers at low Reynolds Number, *Phys. Rev. Lett.* **99**, 228103 (2007).
- [21] G. J. Elfring and E. Lauga, Hydrodynamic Phase Locking of Swimming Microorganisms, *Phys. Rev. Lett.* **103**, 088101 (2009).
- [22] C. Brennen and H. Winet, Fluid mechanics of propulsion by cilia and flagella, *Annu. Rev. Fluid Mech.* **9**, 339 (1977).
- [23] L. N. Wickramaratna, C. Noss, and A. Lorke, Hydrodynamic trails produced by *Daphnia*: Size and energetics, *PloS One* **9**, e92383 (2014).
- [24] T. Kiørboe, H. Jiang, and S. P. Colin, Danger of zooplankton feeding: The fluid signal generated by ambush-feeding copepods, *Proc. R. Soc. B* **277**, 3229 (2010).
- [25] S. Wang and A. Ardekani, Inertial squirmer, *Phys. Fluids* **24**, 101902 (2012).
- [26] N. G. Chisholm, D. Legendre, E. Lauga, and A. S. Khair, A squirmer across Reynolds numbers, *J. Fluid Mech.* **796**, 233 (2016).
- [27] G. Li, A. Ostace and A. M. Ardekani, Hydrodynamic interaction of swimming organisms in an inertial regime, *Phys. Rev. E* **94**, 053104 (2016).
- [28] R. Ouillon, I. A. Houghton, J. O. Dabiri, and E. Meiburg, Active swimmers interacting with stratified fluids during collective vertical migration, *J. Fluid Mech.* **902**, A23 (2020).
- [29] S. MacIntyre, A. L. Alldredge, and C. C. Gotschalk, Accumulation of marines now at density discontinuities in the water column, *Limnol. Oceanogr.* **40**, 449 (1995).

- [30] H. Yamazaki and K. D. Squires, Comparison of oceanic turbulence and copepod swimming, *Marine Ecol. Progress Ser.* **144**, 299 (1996).
- [31] A. L. Alldredge, T. J. Cowles, S. MacIntyre, J. E. Rines, P. L. Donaghay, C. F. Greenlaw, D. Holliday, M. M. Dekshenieks, J. M. Sullivan, and J. R. V. Zaneveld, Occurrence and mechanisms of formation of a dramatic thin layer of Marine snow in a shallow pacific fjord, *Marine Ecol. Progress Ser.* **233**, 1 (2002).
- [32] S. Wang and A. M. Ardekani, Biogenic mixing induced by intermediate Reynolds number swimming in stratified fluids, *Sci. Rep.* **5**, 17448 (2015).
- [33] R. More and S. Balasubramanian, Mixing dynamics in double-diffusive convective stratified fluid layers, *Curr. Sci.* **114**, 1953 (2018).
- [34] A. M. Ardekani and R. Stocker, Stratlets: Low Reynolds Number point-force Solutions in a Stratified Fluid, *Phys. Rev. Lett.* **105**, 084502 (2010).
- [35] J. S. Guasto, R. Rusconi, and R. Stocker, Fluid mechanics of planktonic microorganisms, *Annu. Rev. Fluid Mech.* **44**, 373 (2012).
- [36] A. Doostmohammadi, R. Stocker, and A. M. Ardekani, Low-Reynolds-number swimming at pycnoclines, *Proc. Natl. Acad. Sci.* **109**, 3856 (2012).
- [37] R. Dandekar, V. A. Shaik, and A. M. Ardekani, Swimming sheet in a density-stratified fluid, *J. Fluid Mech.* **874**, 210 (2019).
- [38] R. V. More and A. M. Ardekani, Motion of an inertial squirmer in a density stratified fluid, *J. Fluid Mech.* **905**, A9 (2020).
- [39] C. Noss and A. Lorke, Direct observation of biomixing by vertically migrating zooplankton, *Limnol. Oceanogr.* **59**, 724 (2014).
- [40] I. A. Houghton, J. R. Koseff, S. G. Monismith, and J. O. Dabiri, Vertically migrating swimmers generate aggregation-scale eddies in a stratified column, *Nature (London)* **556**, 497 (2018).
- [41] D. Viličić, T. Legović, and V. Žutić, Vertical distribution of phytoplankton in a stratified estuary, *Aquatic Sci.* **51**, 31 (1989).
- [42] P. Hershberger, J. Rensel, A. Matter, and F. Taub, Vertical distribution of the chloromonad flagellate heterosigma carterae in columns: Implications for bloom development, *Can. J. Fish. Aquat. Sci.* **54**, 2228 (1997).
- [43] R. Glowinski, T.-W. Pan, T. I. Hesla, D. D. Joseph, and J. Periaux, A fictitious domain approach to the direct numerical simulation of incompressible viscous flow past moving rigid bodies: Application to particulate flow, *J. Comput. Phys.* **169**, 363 (2001).
- [44] A. M. Ardekani, S. Dabiri, and R. H. Rangel, Collision of multi-particle and general shape objects in a viscous fluid, *J. Comput. Phys.* **227**, 10094 (2008).
- [45] A. M. Ardekani and R. H. Rangel, Numerical investigation of particle-particle and particle-wall collisions in a viscous fluid, *J. Fluid Mech.* **596**, 437 (2008).
- [46] A. Doostmohammadi, S. Dabiri, and A. M. Ardekani, A numerical study of the dynamics of a particle settling at moderate Reynolds numbers in a linearly stratified fluid, *J. Fluid Mech.* **750**, 5 (2014).
- [47] W. Aniszewski, T. Arrufat, M. Cialesi-Esposito, S. Dabiri, D. Fuster, Y. Ling, J. Lu, L. Malan, S. Pal, R. Scardovelli, and G. Tryggvason, Parallel, Robust, Interface Simulator (PARIS) [arXiv:2012.11744](https://arxiv.org/abs/2012.11744).
- [48] B. P. Leonard, A stable and accurate convective modeling procedure based on quadratic upstream interpolation, *Comput. Methods Appl. Mech. Eng.* **19**, 59 (1979).
- [49] M. Lighthill, On the squirming motion of nearly spherical deformable bodies through liquids at very small Reynolds numbers, *Commun. Pure Appl. Math.* **5**, 109 (1952).
- [50] J. R. Blake, A spherical envelope approach to ciliary propulsion, *J. Fluid Mech.* **46**, 199 (1971).
- [51] T. Pedley, Spherical squirmers: Models for swimming microorganisms, *IMA J. Appl. Math.* **81**, 488 (2016).
- [52] V. Magar, T. Goto, and T. Pedley, Nutrient uptake by a self-propelled steady squirmer, *Quarter. J. Mech. Appl. Math.* **56**, 65 (2003).
- [53] T. Ishikawa and T. Pedley, The rheology of a semi-dilute suspension of swimming model micro-organisms, *J. Fluid Mech.* **588**, 399 (2007).
- [54] J.-L. Thiffeault and S. Childress, Stirring by swimming bodies, *Phys. Lett. A* **374**, 3487 (2010).
- [55] L. Zhu, E. Lauga, and L. Brandt, Self-propulsion in viscoelastic fluids: Pushers vs. pullers, *Phys. Fluids* **24**, 051902 (2012).
- [56] G.-J. Li, A. Karimi, and A. M. Ardekani, Effect of solid boundaries on swimming dynamics of microorganisms in a viscoelastic fluid, *Rheol. Acta* **53**, 911 (2014).
- [57] G.-J. Li and A. M. Ardekani, Hydrodynamic interaction of microswimmers near a wall, *Phys. Rev. E* **90**, 013010 (2014).
- [58] S. Wang and A. Ardekani, Unsteady swimming of small organisms, *J. Fluid Mech.* **702**, 286 (2012).
- [59] A. E. Walsby, Gas vesicles, *Microbiol. Molec. Biol. Rev.* **58**, 94 (1994).
- [60] T. A. Villareal and E. Carpenter, Buoyancy regulation and the potential for vertical migration in the oceanic cyanobacterium trichodesmium, *Microb. Ecol.* **45**, 1 (2003).
- [61] C. Boyd and D. Gradmann, Impact of osmolytes on buoyancy of marine phytoplankton, *Marine Biol.* **141**, 605 (2002).
- [62] F. J. Sartoris, D. N. Thomas, A. Cornils, and S. B. S. Schiela, Buoyancy and diapause in antarctic copepods: The role of ammonium accumulation, *Limnol. Oceanogr.* **55**, 1860 (2010).
- [63] N. K. Sanders and J. J. Childress, Ion replacement as a buoyancy mechanism in a Pelagic Deep-Sea crustacean, *J. Expt. Biol.* **138**, 333 (1988).
- [64] J. Luo, P. B. Ortner, D. Forcucci, and S. R. Cummings, Diel vertical migration of zooplankton and mesopelagic fish in the Arabian sea, *Deep Sea Res., Part II* **47**, 1451 (2000).
- [65] D. K. Steinberg, B. A. Van Mooy, K. O. Buesseler, P. W. Boyd, T. Kobari, and D. M. Karl, Bacterial vs. zooplankton control of sinking particle flux in the ocean's twilight zone, *Limnol. Oceanogr.* **53**, 1327 (2008).
- [66] N. Hill and T. Pedley, Bioconvection, *Fluid Dyn. Res.* **37**, 1 (2005).
- [67] See Supplemental Material at <http://link.aps.org/supplemental/10.1103/PhysRevE.103.013109> for the videos of a colliding pair of pushers and pullers in a stratified fluid.
- [68] J. Towns, T. Cockerill, M. Dahan, I. Foster, K. Gaither, A. Grimshaw, V. Hazlewood, S. Lathrop, D. Lifka, G. D. Peterson *et al.*, XSEDE: Accelerating scientific discovery, *Comput. Sci. Eng.* **16**, 62 (2014).